A brush-based thermo-physical tyre model and its effectiveness in handling simulation of a Formula SAE vehicle

Ozdemir Ozerem and Denise Morrey*

Department of Mechanical Engineering and Mathematical Sciences, Oxford Brookes University, United Kingdom

Abstract

The ability to model tyre dynamics precisely is often one of the most critical elements for realistic vehicle dynamics control and handling investigations. The industry-standard empirical models are able to predict the important tyre forces accurately over a short range of vehicle operating conditions, which is often restricted to the operating conditions experienced during the tyre testing process. In this paper an alternative and practical method to model Formula SAE tyres has been proposed and studied in a series of possible running scenarios. A simple, analytically-solved brush type tyre model is considered for the physical part with the introduction of a novel approach for defining the contact length formulation that incorporates the influence of inflation pressure, camber angle and velocity while a set of ordinary differential equations are employed to predict the thermal behaviour of the tyre model, which are mostly based on an already-existing method that has not been experimentally validated before. The resulting tyre models provide realistic and informative behaviour of the tyre, which has the ability to consider the majority of the typical operating conditions experienced on a FSAE vehicle. The performance of the proposed tyre models are compared against experimental tyre test data, which show good agreement and indicates that the tyre models have the ability to give realistic predictions of the tyre forces and thermal behaviour in the case of thermal tyre model. Furthermore, the temperature-dependent tyre model has been incorporated into a two-track model of Oxford Brookes Racing's Formula SAE vehicle to study the effectiveness of the tyre model during transient handling simulation. The resulting simulations suggest that the proposed tyre model has the ability to represent realistic operating conditions of tyres, and also that tyre temperatures influence the vehicle dynamic behaviour significantly during on-limit scenarios.

Keywords Tyre, dynamics, modelling, physical, thermal, vehicle, handling, simulation, FSAE

***Corresponding author:** Department of Mechanical Engineering and Mathematical Sciences, Oxford Brookes University, Wheatley Campus, Oxford OX33 1HX, United Kingdom. Email: dmorrey@brookes.ac.uk

Introduction

The only component of a vehicle which provides contact with the road surface, and transmits the forces and moments required for vehicle control are the tyres. Hence, the tyres are one of the most important components of a vehicle. However, there is still no theory that has the ability to accurately and faithfully describe tyre behaviour (Pacejka, 2012). As a result, tyre modelling plays a critical role in vehicle dynamics research, control and simulation studies.

Existing tyre models can be categorised into; empirical, semi-empirical, and physical modelling approaches. The empirical type tyre models such as variations of '*Magic Formula*' (Pacejka, 2012) are often regarded as the industry-standard tyre models for handling simulations. These curve-fitting type tyre models provide a robust tool to accurately describe the tyre dynamics of passenger type vehicles, where the tyres are not operated at extreme and wide range of operating conditions during the laboratory or outdoor testing procedures. However, it is acknowledged that these tyre models fail to describe tyre behaviour satisfactorily in extreme scenarios, such as motorsport (Grob, Blanco-Hauge and Spetler, 2015), where the tyre temperature and sliding speed characteristics are significantly different and often highly changing. On the other hand, the physical tyre models with simple modelling approaches allow easy computation, but also lack accuracy. In contrast, more advanced and complex physical modelling techniques provide very good accuracy, but require great computational power and detailed description of the tyre. In addition, the complex physical modelling approach does not easily allow interaction with real-time applications, as is often required in the current lap time simulation tools and race simulators. Moreover, published work in literature focussing on the effects of tyre temperatures on vehicle dynamics is quite limited and would benefit from further investigation.

The aim of this paper is to apply basic tyre modelling methods to develop a practical, robust and efficient physical tyre model which follow analytical solutions, and to extend the physical model using thermal tyre modelling methods, which were not previously validated using experimental data, with further improvements in order to develop a thermo-physical tyre model suitable for Formula SAE vehicle simulations and experimental validation of the developed tyre models.

Basic tyre modelling methods

A physical tyre model, such as the Brush model (Pacejka, 2012), offers a good platform for tyre model development as it utilises numerical and analytical methods. The use of rather simplistic assumptions to characterise the contact patch dimensions, frictional mechanism and bristle properties, such as adopting a constant value over a range of different operating conditions, creates an unrealistic tyre model with poor performance. Work by Sorniotti and Velardocchia (2008) and Kelly and Sharp (2012) attempts to model more realistic brush tyre models. Sorniotti and Velardocchia investigated the behaviour of tyre tread elements by using a brush model with parabolic contact pressure distribution, which incorporates anisotropic stiffness properties, and have outlined the potential improvements for a brush model based on bristle and contact patch characteristics. The model provided good correlation with experimental data (Sorniotti and Velardocchia, 2008). Kelly and Sharp used an isotropic brush model with an arbitrary contact pressure distribution. They incorporated a more realistic frictional mechanism between the road surface and the tyre rubber. Finally, they considered simple mechanisms for the tyre thermal behaviour to derive a set of ordinary differential equations to predict the temperature changes in the tyre. Although they have proposed a great amount of theoretical work with the model, the model has not been compared against experimental data (Kelly and Sharp, 2012). Sorniotti also proposed a semi-empirical method to predict the tyre temperatures and incorporated the effects in a brush model (Sorniotti, 2009). The model was based on an extension to the earlier tyre model developed with Velardocchia (2008).

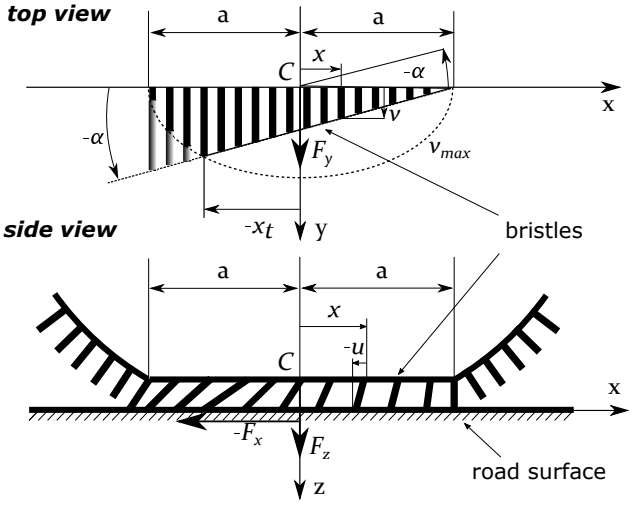

Figure 1: Brush model behaviour in pure lateral (top view) and braking conditions (side view)(Figure adapted from (Pacejka, 2012)).

Figure 1 depicts the brush model concept. In the

brush tyre model theory, the tyre is considered to consist of bristles that represent the tyre tread, which are attached to the tyre belt. The carcass is responsible for supporting the tread and consequently, the bristles. In most of the traditional forms of brush model, the carcass is assumed to be a rigid element. The combination of compliance between these components determines the elasticity of the actual tyre (Pacejka, 2012). As the tyre rolls, the bristles pass through the tyre contact patch area, and are allowed to deflect, due to the driving motion which generates adhesive forces at the road surface. The bristles are deflected in the contact patch until the local friction force can no longer withstand any further shear deformation and transitions into a sliding state over the road surface (Kelly and Sharp, 2012). The combination of the shear forces arising from the adhesive and sliding regions determines the overall tyre forces.

The traditional form of Brush model, as proposed by Pacejka (2012), is used as the reference mathematical frame for the physical tyre model described in this paper. The sign convention used in this work is shown in Figure 2, which follows SAE conventions (Pacejka, 2012). A combined slip approach is employed as the tyre is known to operate at its maximum potential in motorsport, and is expected to be in a combined state of simultaneous lateral and longitudinal deflections. The main assumption of the tyre model is the parabolic pressure distribution across the tyre contact patch. According to Kim and Savkoor (1997), this is the case when small vertical loads are considered. Hence, as low vertical loads (up to ∼2 kN) are usually experienced with the FSAE vehicles, this seems to be a reasonable assumption for this application and makes the solution of the tyre forces simpler by providing analytical solutions (Pacejka, 2012). The bristles are assumed to respond differently to lateral and longitudinal deflections, so that the tyre is assumed to have anisotropic stiffness and frictional properties. Lastly, the bristles are assumed to have identical characteristics along the contact patch length.

Brush model mathematical formulation

The practical quantities of the longitudinal slip, κ, and the slip angle, α, do not allow for a reliable solution in combined slip conditions. According to Pacejka (2012) these quantities are normalised by representing the parameters σ_x and σ_y as the individual theoretical slip quantities for the longitudinal and lateral directions, which are given by (Pacejka, 2012):

$$\sigma_x = \frac{\kappa}{1+\kappa}, \qquad \sigma_y = \frac{\tan\alpha}{1+\kappa} \tag{1}$$

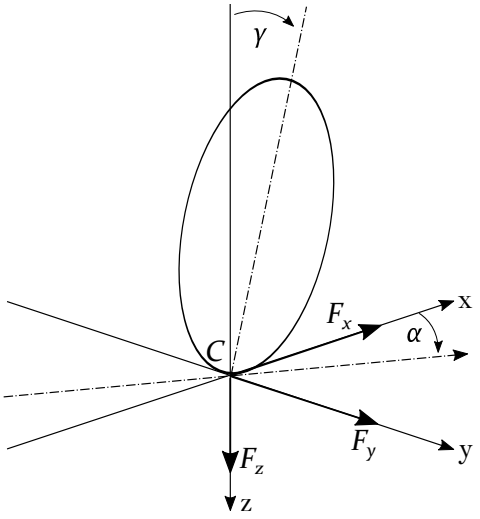

Figure 2: SAE tyre sign conventions.

Effects of ply-steer are also incorporated in this work as built-in slip angle (Pacejka, 2012).

The resultant theoretical slip, σ, of the tyre in the combined slip conditions can then be given as:

$$\sigma = \sqrt{{\sigma_x}^2 + {\sigma_y}^2} \tag{2}$$

These slip quantities affect the longitudinal and lateral deflections of the bristles within the contact patch, based on position of a tread element along the contact patch length, x, and half the contact patch length, a, as depicted in Figure 1. Within the adhesion region, static frictional forces apply to the bristles which cause deflection in both longitudinal and lateral directions (u and v) depending on tyre slip conditions. These deflections are represented respectively as (Pacejka, 2012):

$$u = (\mathrm{a} - x)\sigma_x, \qquad v = (\mathrm{a} - x)\sigma_y \tag{3}$$

The deflections of the bristles are the main contributors to the shear forces generated at the adhesion region of the contact patch. Therefore, the longitudinal and the lateral contact forces per unit length (q_x and q_y) within the adhesion region can be expressed by assuming that the bristles behave as linear springs with anisotropic stiffnesses (k_{px} and k_{py}):

$$q_x = k_{px}u, \qquad q_y = k_{py}v \tag{4}$$

The tyre longitudinal and lateral forces for an assumedly rectangular contact patch shape with length 2a and width 2b for complete adherence with the road

surface can then be given by integrating the contact forces over the contact patch area:

$$F_x = \int_{-\mathrm{b}}^{\mathrm{b}} \int_{-\mathrm{a}}^{\mathrm{a}} q_x \, dx \, dy$$
$$F_y = \int_{-\mathrm{b}}^{\mathrm{b}} \int_{-\mathrm{a}}^{\mathrm{a}} q_y \, dx \, dy \tag{5}$$

Analytical solution to the equations (5) for null tyre slip conditions then gives the longitudinal stiffness and cornering stiffness expressions of the tyre:

$$C_{F\kappa}\Big(\frac{\partial F_x}{\partial \kappa}\Big)_{\kappa=0} = 4\mathrm{a}^2\mathrm{b}k_{px}$$
$$C_{F\alpha}\Big(\frac{\partial F_y}{\partial \alpha}\Big)_{\alpha=0} = 4\mathrm{a}^2\mathrm{b}k_{py} \tag{6}$$

In this work, the longitudinal stiffness and cornering stiffness of the tyre follow empirical definitions (Smith, 2003), which are given by:

$$C_{F\kappa} = C_{F\kappa 0} \cdot dF_z e^{-c_{cfx}(dF_z - 1)}$$
$$C_{F\alpha} = C_{F\alpha 0} \cdot dF_z e^{-c_{cfy}(dF_z - 1)} \tag{7}$$

where $C_{F\kappa 0}$ and $C_{F\alpha 0}$ are the reference longitudinal and cornering stiffnesses of the tyre, respectively. The use of an exponential type empirical law for defining the longitudinal and cornering stiffnesses of the tyre eliminates poor extrapolation performance of the model at higher vertical loads, unlike the bevahivour of the linear fit (Sorniotti and Velardocchia, 2008) or polynomial type empirical models. The fitted coefficients c_{cfx} and c_{cfy} determine the magnitude of change in longitudinal and cornering stiffnesses in relation to the vertical load variation acting on the tyre. The vertical load ratio dF_z is given by:

$$dF_z = \frac{F_z}{F_{z0}} \tag{8}$$

where F_z is the vertical load acting on the tyre, while F_{z0} is the reference or nominal vertical load. The model behaviour against measured data in the lateral direction for a range of vertical loads is shown in Figure 3, which shows good agreement. Use of equations (6 to 8) then enables to estimate the bristle stiffnesses k_{px} and k_{py} at different vertical loads.

However, the contact patch can no longer be characterised by full adhesion in conditions where the tyre is rolling with the presence of slip and limited friction. Hence sliding commences within the contact patch at the point where the bristle contact forces exceed the limits of the frictional forces available at the road surface. Based on the traditional brush model theory, this

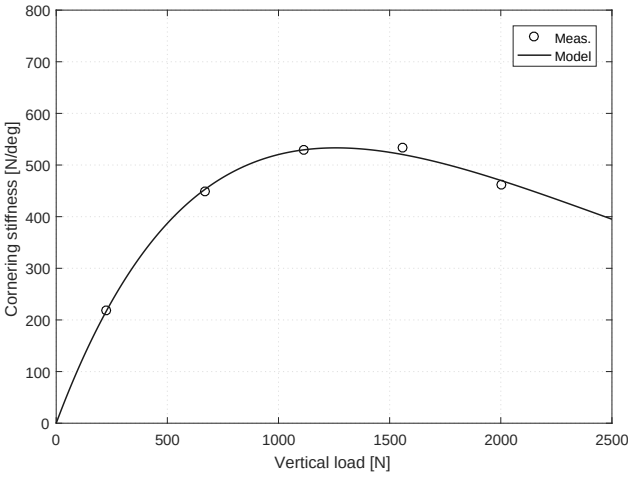

Figure 3: Cornering stiffness model in comparison with measured data (Meas.) at different vertical loads.

occurs when the resultant contact force per unit length exceeds the static frictional limits, and in this work it is assumed that the contact patch is characterised by singular adhesion and sliding regions in order to allow an analytical solution. The transition point, x_t, where contact transitions into the sliding region is determined by solving the following condition:

$$\sqrt{\Big(\frac{k_{px}\sigma_x}{\mu_{sx}}\Big)^2 + \Big(\frac{k_{py}\sigma_y}{\mu_{sy}}\Big)^2}(\mathrm{a} - x_t) = \frac{3F_z}{8\mathrm{ab}}\left\{1 - \Big(\frac{x_t}{\mathrm{a}}\Big)^2\right\} \tag{9}$$

where μ_{sx} and μ_{sy} are the static friction coefficients in the longitudinal and lateral directions, respectively.

Given the contact transition point is known, the tyre forces can then be computed by:

$$F_x = \int_{-\mathrm{b}}^{\mathrm{b}} \int_{x_t}^{\mathrm{a}} q_x \cdot dxdy + \int_{-\mathrm{b}}^{\mathrm{b}} \int_{-\mathrm{a}}^{x_t} \frac{\sigma_x}{\sigma} \mu_{kx} q_z(x) \, dx \, dy$$
$$F_y = \int_{-\mathrm{b}}^{\mathrm{b}} \int_{x_t}^{\mathrm{a}} q_y \cdot dxdy + \int_{-\mathrm{b}}^{\mathrm{b}} \int_{-\mathrm{a}}^{x_t} \frac{\sigma_y}{\sigma} \mu_{ky} q_z(x) \, dx \, dy \tag{10}$$

where μ_{kx} and μ_{ky} are the kinetic friction coefficient in the longitudinal and lateral directions, respectively, and q_z is the contact patch vertical load distribution, which is assumed to have a parabolic shape along the contact patch length with a uniform profile across the width of the contact patch that can be expressed by:

$$q_z = \frac{3F_z}{8\mathrm{ab}}\left\{1 - \Big(\frac{x}{\mathrm{a}}\Big)^2\right\} \tag{11}$$

Coefficient of friction characterisation

Sharp, Gruber and Fina (2015) highlight the importance of frictional forces at the contact patch by stating

that the tyre forces mainly depend on the friction between the tread rubber and the road surface. The physical phenomena which generate the frictional forces are, however, significantly complex. The frictional forces are generally influenced by factors such as road surface and texture (micro and macro roughness), surface temperatures of the road and the tread rubber, and the sliding speed of the tread rubber (Sharp, Gruber and Fina, 2015). Therefore, the typical approach of assuming a Coulomb's friction law on rubber friction, which uses constant values of static and kinetic coefficients of friction between the tyre and the road surface, is an ineffective way of accurately characterising the frictional forces. Moreover, according to Mavros (2009), the sliding speed of the tyre is known to have a significant influence on the magnitude and behaviour of the kinetic friction coefficient of the tyre. For instance, Pacejka (2012) uses a linear, velocity-dependent model for simulating the friction behaviour of a bristle element, by approximating this to the sliding speed of the tyre belt, as the tyre rolls over the ground surface. Nevertheless, this is a relative simplification, as the effects of bristle temperatures are neglected, and due to the fact that in reality the friction decay with increasing sliding speed can be non-linear. As mentioned earlier, another influence on the tyre rubber and the road surface friction is directly related to temperature. Earlier work by Kelly and Sharp (2012) proposed an empirical formulation to describe a master curve for the characterisation of the kinetic coefficient of friction between the rubber and the road surface, which was implemented in determining the frictional characteristics of the proposed tyre model in this work. The equation is a modified Savkoor-type empirical rubber friction model (Mavros, 2009), which is a function of both the sliding speed of the bristles' tips over the road surface and the surface temperature of the tyre tread. Shape factors $c_{\mu vs}$ and $c_{\mu t}$ are included in this exponential decay type model, that is a function of the sliding speed components in longitudinal or lateral directions, $V_{sx,y}$, the difference between tread temperature, T_t, and the reference temperature, T_0, in addition to the pre-defined limits of minimum and maximum values of the friction coefficient (μ_0 and μ_m). The kinetic friction coefficient in the longitudinal and lateral directions can be expressed by (Kelly and Sharp, 2012):

$$\begin{aligned}\mu_{kx} &= \mu_0 + (\mu_m - \mu_0)e^{-[c_{\mu vs}(log_{10}(V_{sx}))-c_{\mu t}(T_t-T_0)]^2} \\ \mu_{ky} &= \mu_0 + (\mu_m - \mu_0)e^{-[c_{\mu vs}(log_{10}(V_{sy}))-c_{\mu t}(T_t-T_0)]^2}\end{aligned} \tag{12}$$

In this work, the sliding speed used in determining the coefficient of friction is approximated to be equal to the slip velocity at the tyre contact centre, as a result of the rigid carcass assumption. However, in reality the sliding speed of the tyre rubber varies along the sliding region of the contact patch, which may show variations in local friction coefficient, and potentially influence the frictional power associated with the sliding. The model proposed in this work considers steady-state deflection of bristles in the sliding region, which considers the slip speed to be equal to the sliding speed (Pacejka and Sharp, 1991), an assumption taken in order to allow full analytical solution to the tyre forces given by equation 10, hence neglecting the localised dynamic effects. The effect of temperature and sliding speed on the kinetic friction coefficient for a typical Formula SAE tyre tread compound, solved using equation (12) and generic values is depicted in Figure 4. Increasing the temperature of the rubber leads to a horizontal shift of the peak friction coefficient. Similarly, Figure 5 shows the sliding speed dependency of the kinetic friction coefficient across different tyre operating temperatures. The temperature effects are ignored for the steady-state non-thermal model.

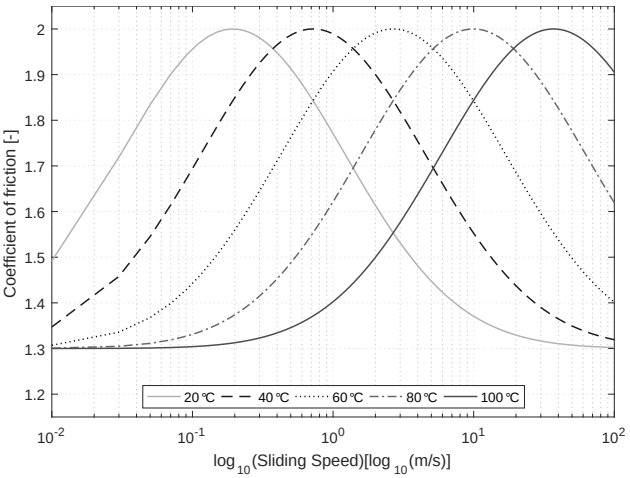

Figure 4: Variation of kinetic friction coefficient with respect to bristle sliding speed for a range of temperatures.

In addition, the reduction in friction coefficient as a result of increasing contact pressure is accounted for using a linear relationship (Kelly and Sharp, 2012). The reduction factor, C_{cp}, is given by:

$$C_{cp} = 1 - c_{\mu cp} \cdot dP_{cp} \tag{13}$$

where dP_{cp} is the global contact patch pressure ratio and the magnitude of reduction is hence controlled by the coefficient, $c_{\mu cp}$. The global contact patch pressure ratio is given by:

$$dP_{cp} = \frac{P_{cp}}{P_{cp0}} \tag{14}$$

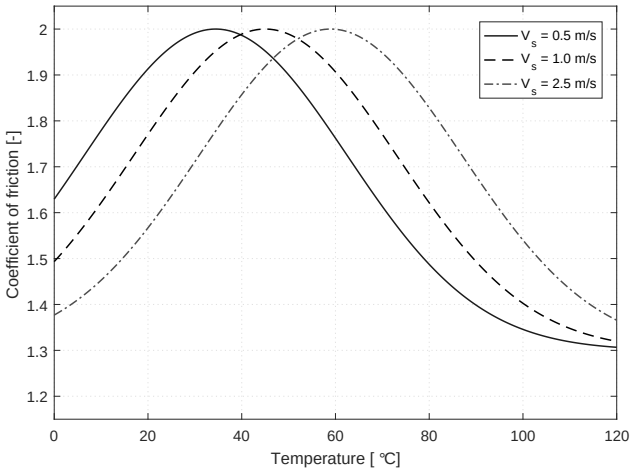

Figure 5: Influence of sliding speed on kinetic friction coefficient.

where P_{cp} is the global contact patch pressure and P_{cp0} is the reference global contact patch pressure value. The reduction factor, C_{cp}, is then used to determine the actual static and kinetic friction coefficients in the longitudinal or lateral directions ($\mu_{sx,y}$ and $\mu_{kx,y}$) using (Kelly and Sharp, 2012):

$$\begin{aligned} \mu_{sx,y} &= \mu_{sx,y} \cdot C_{cp} \\ \mu_{kx,y} &= \mu_{kx,y} \cdot C_{cp} \end{aligned} \tag{15}$$

Contact patch geometry

The boundaries for the contact patch length are significant for determining the forces generated at the contact patch, as indicated by equation (10). Furthermore, the contact patch length is also responsible for determining the position of the adhesion to sliding transition point, x_t. Based on experimental observations of the authors using a glass rig test bench, in another study, the length of the contact patch was found to be more sensitive to the vertical load intensity than the contact patch width, which was also found to show a small variation for typical FSAE tyres (Ozerem, 2014). Hence, the contact patch width is assumed to have a constant value in the present work for simplicity reasons, that is $w_{cp} = 2\text{b}$, where w_{cp} is the nominal tyre tread width. The contact patch is also assumed to be rectangular. For slick-type racing tyres, there is no need to specify a grooving or cut-out rate of the tread pattern and the total contact patch area can be assumed to be in a complete contact with the road surface. However, estimation of the tyre contact patch dimensions are fairly complex due to a number of reasons, such as the influence of cornering forces, camber angle and conditions of under-inflation or over-inflation. An experimental procedure for determining the contact patch dimensions would offer a precise method of empirical contact patch size determination (Ozerem, 2014). Unfortunately this type of testing is highly complex and would justify a single, more detailed study on its own right, and is outside the scope of this particular paper. Consequently, a simple theoretical method proposed by Gim (1988), that is based on the Pythagorean theorem, is adopted in this work to determine the contact patch length, l_{cp}, and half contact patch length, a:

$$l_{cp} = 2\text{a}, \qquad \text{a} = \sqrt{{R_0}^2 - (R_0 - \delta_z)^2} \tag{16}$$

Hence in this expression the contact patch length is related to the unloaded radius, R_0, and vertical deflection of the tyre, δ_z. The vertical deflection of the tread is directly proportional to the vertical load acting on the tyre and tyre vertical stiffness, K_z. Although the tyre vertical stiffness is usually assumed to have a constant value, analysis of the behaviour of a rolling tyre during vertical testing shows (Avon Motorsport, 2015) that the vertical stiffness is dependent on several factors, primarily the inflation pressure, camber angle and angular velocity of the tyre:

$$\delta_z = \frac{F_z}{K_z}, \quad K_z = f(P_i, \gamma, \omega) \tag{17}$$

Assuming that the tyre responds linearly to these parameters, the following new formulation of a tyre vertical stiffness equation is derived, based on a linear-fit of empirical data:

$$K_z = K_{z0}\{[1-(P_{i0}-P_i)\lambda_i]\cdot[1-\gamma\lambda_g]\cdot[1-\omega\lambda_{av}]\} \tag{18}$$

where K_{z0} is the reference vertical stiffness, P_{i0} is the reference inflation pressure, P_i is the inflation pressure, ω is the angular velocity and γ is the camber angle of the tyre. Lastly, the parameters λ_i, λ_g and λ_{av} are used to represent the coefficients of a real life tyre's response to the inflation pressure, camber angle and angular velocity respectively, but they require specific experimental data to be determined. This simple and linear description of the vertical tyre stiffness, however, does not take into account the dynamic behaviour or temperature-related effects of the tyre. Nevertheless, it attempts to consider the important parameters which affect the vertical stiffness of a tyre, as it rolls on a flat surface.

Model parameter estimation

The model parameters are estimated using a constrained non-linear optimisation routine that minimises the least square error between the measured tyre force data and the simulated tyre behaviour. For the physical tyre model, which neglects the temperature effects, a total number of 20 parameters need to be estimated that accounts for the pure longitudinal, pure lateral and combined slip conditions. This a significant improvement over the Magic Formula tyre models, which have an excessive amount of parameters (Pacejka, 2012).

The physical model proposed above allows solution of tyre force characteristics with constant values of rubber temperature and inflation gas pressure. This type of model offers a reasonable tyre model to be used in vehicle handling simulations, where the temperature changes are not significant, or where steady-state behaviour is of interest. The influence of tyre temperatures and inflation gas pressure variations are accounted with the addition of thermal modelling in the next section.

Physical model experimental validation

The validation of the tyre model output against experimental data is highly important to prove the accuracy of the tyre model estimations. However, access to the experimental data for tyres is often very challenging due to the limited availability of sophisticated tyre testing facilities and resources. Furthermore, for a complete handling type tyre model validation, the tyres need to be tested at a wide range of operating conditions. Avon Motorsport/Cooper Tires 6.2/20.0-13 Formula SAE specification tyres have been modelled in this paper, as used on the Oxford Brookes Racing Team's vehicle in 2014 competitions. According to Kasprzak and Gentz (2006), the 'Formula SAE Tyre Test Consortium (FSTTC)' was found to provide teams competing in the Formula SAE competition with high quality tyre data, necessary for vehicle handling simulations and vehicle development (Kasprzak and Gentz, 2006). The experimental data was measured at the well-known CALSPAN Tire Research Facility in the USA where the tyres are tested at typical operation conditions experienced in the FSAE competitions. The experimental test inputs such as lateral and longitudinal slip, forward velocity, camber angle and vertical load acting on the tyres have been applied to the physical tyre model in order to simulate a virtual tyre test bench. For the physical tyre model, the temperature

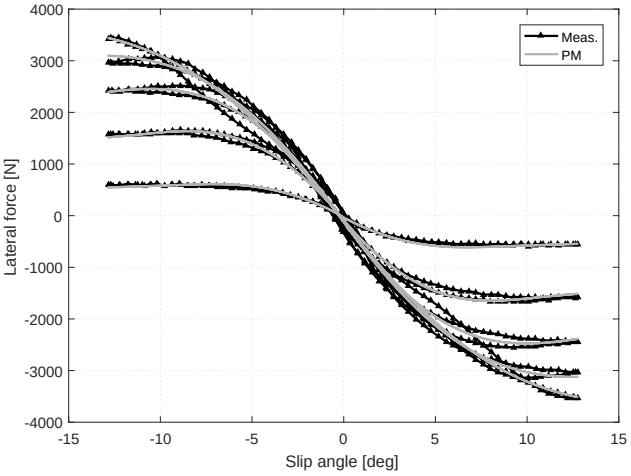

Figure 6: Lateral force behaviour of the physical model (PM) in comparison with measured data (Meas.) as a function of slip angle.

effects are neglected. The 5.2 version of Magic Formula has also been modelled and parametrised in a similar way with the physical model in order to compare the proposed models in this paper against a proven tyre model. As this work is primarily concerned with the cornering performance of a vehicle, the comparison between the models and measured data will only be shown for a pure lateral slip case.

Figure 6 shows the comparison of the outputs from the physical tyre model and measured data for the pure lateral slip test. The physical model is in very good agreement with the measured data across the tested vertical load and slip angle ranges as the average fitting error is 6.19%. On the other hand, Figure 7 shows comparison also with the Magic Formula model, in which the difference between the tyre models is almost indistinguishable. The MF5.2 provides a fitting error of only 0.46% less than the physical model. Therefore, even though the tyre temperature effects are not incorporated, the proposed model performs quite well when compared against both experimental data and the industry-standard Magic Formula for the pure lateral behaviour.

Thermal model

The physical tyre model was extended in order to include the effects of tyre, road surface and surrounding temperatures with the tyre thermal modelling approach proposed by Kelly and Sharp (2012). The model is adopted to a great extent, mainly because

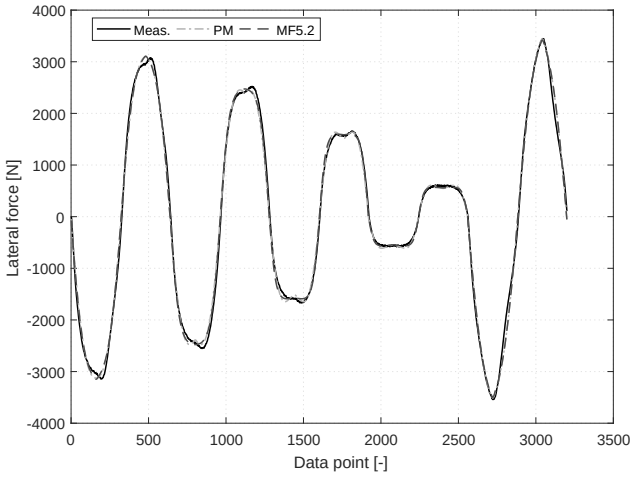

Figure 7: Lateral force behaviour of the physical model (PM) in comparison with measured data (Meas.) and Magic Formula model (MF5.2).

of its degree of fit, and suitability with the physical tyre model proposed in the earlier section.

In this thermal modelling approach, the tyre is assumed to consist of only three bodies for simplification reasons. The main causes of the temperature changes are due to two factors. Firstly, the tyre heating process through work done, and secondly, the heat transfer between tyre bodies, road surface and the ambient surrounding. The temperature throughout the depth of the tread and the carcass are assumed to be uniform. This is also the case across the contact patch area.

Tyre heating process

The primary reasons for tyre heating are based on two factors:

(i) The tyre deforms due to carcass deflection as it passes through the contact patch. This process causes energy dissipation, which contributes to heating of both the tread and the carcass.

(ii) The frictional power acting on the tyre in the sliding region of the contact patch, as the tip of the bristles slide over the road surface.

It is assumed that the deflection of the carcass is directly related to the travelling velocity of the tyre, and the total forces acting on the tyre in the longitudinal, lateral and vertical directions. Efficiency parameters are used in addition to control the amount of heat generation in all directions (Kelly and Sharp, 2012). The deflection power in the longitudinal, lateral and vertical directions are given as:

$$\begin{aligned} Q_{DPx} &= \eta_x V_x |F_x| \\ Q_{DPy} &= \eta_y V_x |F_y| \\ Q_{DPz} &= \eta_z V_x |F_z| \end{aligned} \tag{19}$$

where $Q_{DPi}, i = x, y, z$ and $\eta_i, i = x, y, z$ stands for the deflection power and efficiency terms in the longitudinal, lateral and vertical directions, respectively. The net deflection power can be given by:

$$Q_{DPnet} = Q_{DPx} + Q_{DPy} + Q_{DPz} \tag{20}$$

Simple terms describing the frictional power, Q_{FP}, are used to calculate the tyre heating within the contact patch. In contrast to the model proposed by Kelly and Sharp (2012), the model considers the fact that only a part of the vertical load across the contact patch is carried by the sliding portion of the contact patch. The heating of the contact patch are hence related to the frictional forces arising from the sliding portion of the contact patch and the sliding speed of the tyre tread on the ground surface:

$$Q_{FP} = \Big\{ |V_{sx}| \cdot |F_{x,slide}| + |V_{sy}| \cdot |F_{y,slide}| \Big\} R_{RT} \tag{21}$$

where R_{RT} is a constant which determines the proportion of the heat energy that the tyre receives from this frictional power.

Heat transfer process

The heat transfer processes between the tyre bodies, road and ambient surroundings have a significant effect on overall temperature across the components of tyre. Constant values for the ambient and the road surface temperature are considered here, as the temperature changes of these can be considered as negligible. Simple principles of thermodynamics are used to determine the heat transfer around the tyre bodies. For instance, the tread conducts heat to the road surface in the adhesion region and convects heat to the ambient surroundings, but receives a proportion of the heat generated by the friction power and deflection.

The heat transfer between the road and the ambient surroundings is related to the heat transfer coefficient, h, and the temperature difference between these bodies. The equation is given as:

$$Q_{2-5} = h_{2-5}(T_t - T_a) \tag{22}$$

where T_a indicates the surrounding temperature. $Q_j, j = 1, 2, 3, 4, 5$ and $h_j, j = 1, 2, 3, 4, 5$ are the heat

transfer rate and heat transfer coefficient between road, tread, carcass, inflation gas and ambient, respectively. The heat transfer between the tread and the road surface is given as:

$$Q_{2-1} = h_{2-1}(T_t - T_r) \cdot A_{cp,adhere} \tag{23}$$

where T_r indicates the road surface temperature and $A_{cp,adhere}$ indicates the non-sliding portion of the contact patch area.

The heat transfer between the tread and the carcass is given as:

$$Q_{2-3} = h_{2-3}(T_t - T_c) \tag{24}$$

where T_c indicates the carcass temperature. The carcass also convects heat to the ambient air around the tyre sidewall region, which can be given as:

$$Q_{3-5} = h_{3-5}(T_c - T_a) \tag{25}$$

The heat transfer between inflation gas and the carcass is given as:

$$Q_{3-4} = h_{3-4}(T_c - T_i) \tag{26}$$

where T_i indicates the inflation gas temperature.

Finally, the heat transfer around the inflation gas is much simpler, compared to the tread and carcass, as it depends only on the heat transfer with the carcass. The actual inflation pressure is then calculated using ideal gas law. Several other factors which influence the heat transfer around the tyres in motorsport use, such as heat radiation from brakes, engine, exhaust, wheel rims, road surface or sunlight are neglected due to added complexity in description of accurate thermal surrounding conditions. However, the main factors are considered (Kelly and Sharp, 2012).

Rate of temperature change

The heat generations and heat transfer between the tyre bodies are then used to determine the rate of temperature changes for the tyre. The set of ordinary differential equations to solve the tread, carcass and inflation gas rate of temperature changes are related to the specific heat capacity, c_p, and mass of the bodies, m, and can be expressed by:

$$\begin{aligned} \dot{T}_t &= \frac{Q_{FP} + Q_{DPt} - Q_{2-1} - Q_{2-3} - Q_{2-5}}{c_{p,t} m_t} \\ \dot{T}_c &= \frac{Q_{DPc} + Q_{2-3} - Q_{3-4} - Q_{3-5}}{c_{p,c} m_c} \\ \dot{T}_i &= \frac{Q_{3-4}}{c_{p,i} m_i} \end{aligned} \tag{27}$$

where the subscripts are: tread, t; carcass, c; inflation gas, i. Additionally, the deflection power is distributed between the tread and the carcass using a constant, R_{CT}, which determines the amount of power the tread or the carcass receives:

$$\begin{aligned} Q_{DPt} &= Q_{DPnet} \cdot R_{CT} \\ Q_{DPc} &= Q_{DPnet} \cdot (1 - R_{CT}) \end{aligned} \tag{28}$$

Additionally, the influence of tyre temperature on the linear working range of the tyre is accounted for using a linear drop of cornering stiffness with increasing temperature, similar to the model proposed by Mizuno et al. (2005). As the proposed model is a time-dependent model, the tyre transient properties are accounted for using a first-order approach based on tyre relaxation length (Pacejka, 2012). In this approximation, the lateral relaxation length, τ_y, is defined as:

$$\tau_y = \frac{C_{F\alpha}}{K_y} \tag{29}$$

where K_y is the lateral stiffness of the tyre.

Thermo-physical model experimental validation

The extended physical model with the addition of the thermal model or in other terms, the 'thermo-physical model', has been simulated against the experimental data in an identical virtual tyre test bench using the FSTTC tyre testing inputs, in a similar fashion to the physical model validation described in the earlier section. The parameter estimation firstly involves in identification of the coefficient of friction and cornering stiffness related parameters by fitting the model parameters using the measured lateral force data, similar to the steady-state physical model parameter identification process. Certain empirical-based thermal model parameters are then determined for complete tyre model parameter identification. It should also be noted that the experimental data consisted of discontinues in time and force data points in between slip angle sweeps and hence the full and continuous temperature history of the tyre testing was not available. Therefore, the initial tread temperature of the tyre at the beginning of each sweep is assumed to be equal to the measured data.

Figure 8 and Figure 9 show the results of the thermo-physical model from the virtual test bench in comparison with the experimental test data and demonstrate that the model is able to provide a good estimation in general for both the lateral force and the tread temperature of the tyre. The average fitting error of the

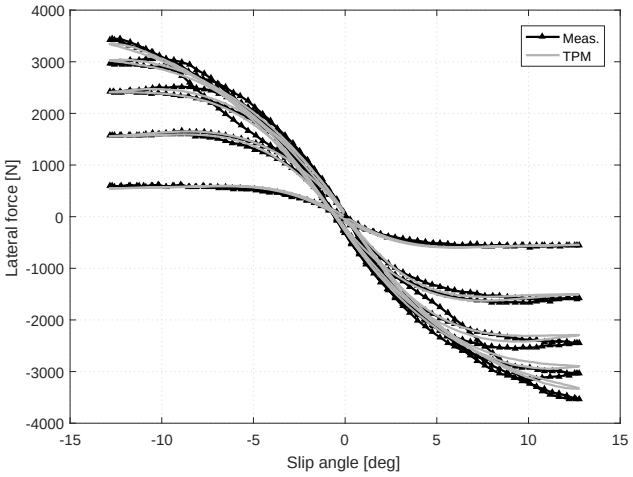

Figure 8: Lateral force behaviour of the thermo-physical model (TPM) in comparison with measured data (Meas.) as a function of slip angle.

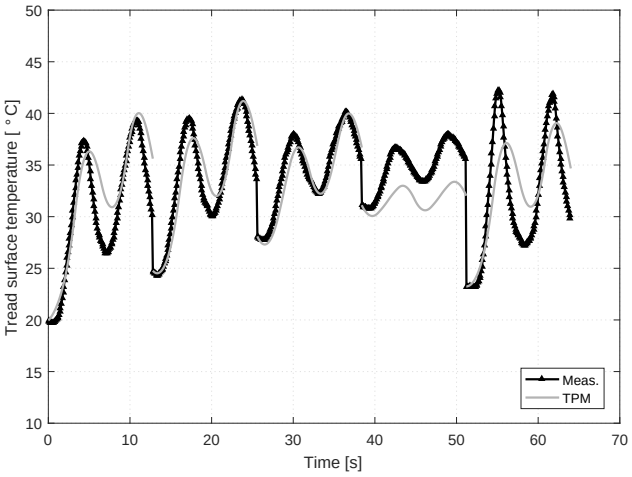

Figure 9: Tyre tread temperature prediction of the thermo-physical model (TPM) in comparison with measured data (Meas.) with respect to time.

thermo-physical model with respect to the measured data is 6.09% for the lateral force and 8.50% for the tread temperature output. In comparison with the physical model experimental correlation shown in Figure 6, the model performance improves by 0.1% on average fitting error and the thermal model has the capability of capturing the hysteresis behaviour at the linear range of the tyre operation at small slip angles due to relaxation effects and at higher slip angles due to frictional changes caused by heating/cooling of the tyre, both of which the physical model is not able to consider. Furthermore, it is shown in Figure 8 that the relaxation length estimation of the model is of good accuracy for different vertical loads and tyre temperatures. Analysing the tyre model's tread temperature estimation (Figure 9), even though the model is based on simple principles and uses significant assumptions, the general trend is of acceptable accuracy. The most significant flaws in performance of the tyre model prediction occur at the lowest and highest vertical loading cases between 38 and 64 seconds, which suggests that either the friction or contact patch size estimation of the tyre model is not able to produce realistic values in such cases. In addition, the cooling behaviour of the model supports the latter observation, as the model is not able to provide a sufficient correlation in temperature during cooling phases of certain vertical loads, which is most likely to be related with the incorrect sizes of adhesive and sliding regions within the contact patch.

Figure 10 shows the model behaviour operating at a higher slip angle range, where the advantage of the thermo-physical model over the physical model is highlighted. It is shown that the thermo-physical model is able to capture the temperature related lateral force change at higher slip angle similar to the the lateral force trend of the measured data, which is not the case when the physical model is simulated. Even though the model is not able to provide a perfect correlation against measured data, resulting simulations of the thermo-physical tyre model suggests that it could provide a useful platform to investigate the tyre temperature related effects in vehicle dynamics studies, especially in motorsport, as it is shown to capture important tyre model behaviour with respect to tyre temperature variations.

Vehicle dynamic simulation

Undoubtedly, the main interest of racing teams is to improve vehicle performance. The best practice in achieving improved lap times is usually through analysing computational vehicle simulation for a variety of manoeuvres. As this paper is aimed at investigating and modelling of tyre temperature effects, the thermo-physical tyre model described earlier is incorporated into a transient vehicle model using Oxford Brookes Racing's 2014 FSAE vehicle parameters, and is simulated in a high speed, smooth and low speed, challenging type manoeuvres.

Vehicle model

The vehicle model used in this work is depicted in Figure 11, and is a classical two-track model. The model

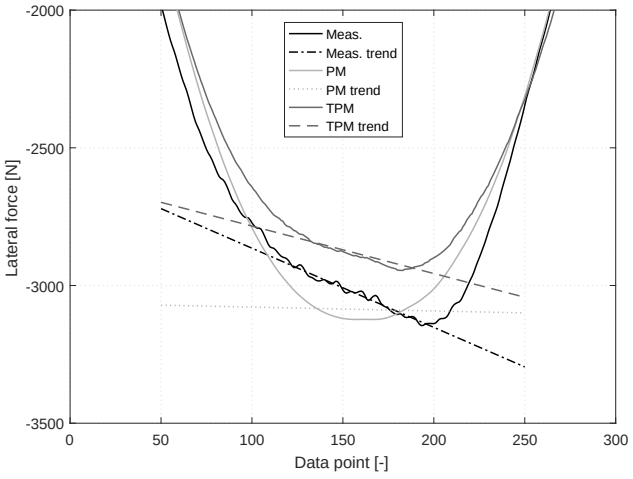

Figure 10: Comparison of lateral force estimation of the physical model (PM) and the thermo-physical model (TPM) against measured data (Meas.) at higher slip angle range.

considers the yaw and lateral degrees of freedom associated with the vehicle movement. A constant forward velocity is applied to specifically study the pure steady state cornering capabilities of the vehicle without considering the longitudinal dynamics involved during manoeuvring. As a two-track model, it also considers the lateral weight transfer between all four wheels through a roll balance distributed between front and rear axles based on quasi-static assumptions. This enables investigation of individual tyre temperatures and tyre behaviour around the vehicle. In addition, a simple aerodynamic model is used to determine the downforce, as a function of vehicle forward velocity, acting on each wheel through a centre of pressure coefficient and a lift coefficient. The aerodynamic balance is biased heavier towards the rear, which provides a higher proportion of the aerodynamic downforce on the rear than the front, with the aerodynamic effects being more significant at higher speeds. The vehicle parameters are given in Table 1. Additionally, the relaxation effects of the tyre are ignored in vehicle simulation in order to generate smoother results.

The vehicle kinematic equations of motion are given as:

$$\begin{aligned} \dot{X} &= \mathrm{u}\cos\psi - \mathrm{v}\sin\psi \\ \dot{Y} &= \mathrm{v}\cos\psi + \mathrm{u}\sin\psi \\ r &= \dot{\psi} \end{aligned} \tag{30}$$

where X and Y are the displacements of the vehicle centre of gravity in the longitudinal and the lateral directions and ψ is the yaw angle of the vehicle. In addition, v and u are the vehicle centre of gravity velocities in the lateral and longitudinal directions, respectively.

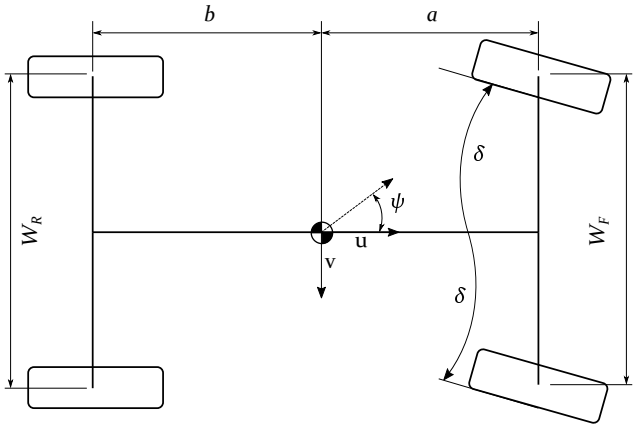

Figure 11: Representation of a two-track vehicle model.

Table 1: Vehicle model parameters.

Parameters	Symbol	Value	Unit
Gravitational acceleration	g	9.81	$\mathrm{m/s^2}$
Vehicle mass	m_v	238	kg
CG height	h_{CG}	0.28	m
Wheelbase	l	1.6	m
CG to front axle distance	a	0.83	m
CG to rear axle distance	b	0.77	m
Yaw moment of inertia	I_z	75	$\mathrm{kgm^2}$
Front track width	W_F	1.21	m
Rear track width	W_R	1.2	m

CG: centre of gravity.

The vehicle dynamic equations of motion are given as:

$$\begin{aligned} m_v(\dot{\mathrm{v}} + \mathrm{u}r) &= F_{y,FL} + F_{y,FR} + F_{y,RL} + F_{y,RR} \\ I_z\dot{r} &= a(F_{y,FL} + F_{y,FR}) - b(F_{y,RL} + F_{y,RR}) \end{aligned} \tag{31}$$

Vehicle control

As the forward velocity of the vehicle is fixed at a constant value, the only control on the vehicle is through the steering input acting on the front wheels. A parallel steering geometry is assumed so that both of the front wheels steer at the same rate, which ignores the effects of Ackermann steering. A non-linear steering controller proposed by Sharp, Casanova and Symonds (2000) is used in calculation of the steering input, δ,

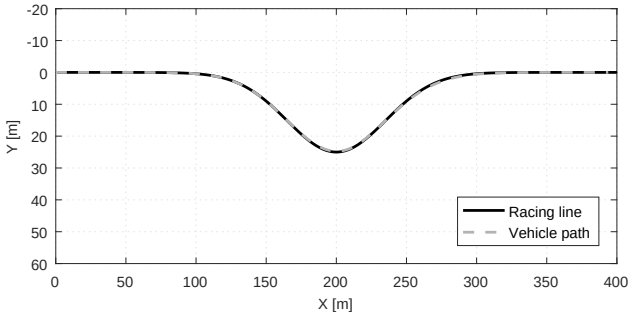

Figure 12: Position of the vehicle during lane change manoeuvre.

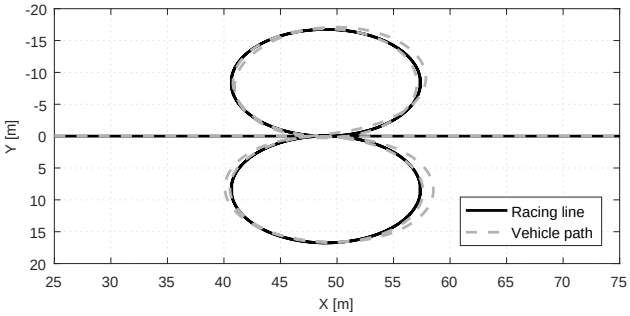

Figure 13: Position of the vehicle during skid-pad event.

required to follow the desired trajectory line. The controller gets sample values of preview path information, $e_{i:n}$, current lateral off-set error, e_1, and angular position error, e_ψ and through a set of individual control gains, K, calculates the required steering angle. The steering control input is given as (Sharp, Casanova and Symonds, 2000):

$$\delta = K_\psi e_\psi + K_1 e_1 + \sum_{i=2}^{n} K_i e_i \tag{32}$$

Vehicle performance

The vehicle model is simulated for two different scenarios. The first one is a high speed and smooth lane change manoeuvre (Brayshaw, 2004). The second event is a typical Formula SAE competition skid-pad event (Formula SAE Online, 2016), which is lower speed but consists of challenging cornering events with tight cornering radii. The racing line for both scenarios has been generated based on the curvature profile along the desired trajectory.

The lane change manoeuvre consists of two straight sections, two right corners and a tight left corner section. The skid-pad event consists of a short straight and two initial turns to the right direction followed by a transition to left turns for two times, before the final short straight section. The vehicle forward velocity was set to 28 m/s and 10 m/s for the lane change and the skid-pad simulations, respectively. The path following ability of the vehicle model is shown in Figure 12 for the lane change manoeuvre and in Figure 13 for the skid-pad event. The vehicle is able to follow the desired racing line with good accuracy as the distance from the vehicle centre of gravity to the desired path does not exceed around 1 m in either of these simulations.

The resulting tyre tread temperatures from simulation along vehicle trajectory for both events are shown in Figure 14. Although the variation in temperatures is quantitatively not very high, analysing the temperature profile shows that the tyre model follows the expected behaviour. For instance, the temperature drops while travelling on the straight sections, mainly due to lack of tyre slip. As the vehicle turns into the first corner of the lane change manoeuvre (Figure 14a), the tread temperatures rise at an identical rate, however as the vehicle negotiates the much tighter corner, the tyre temperatures rise up with different rates in relation to each other. This is related to the presence of increased weight transfer at higher lateral accelerations (Figure 15a). Consequently, the tyre temperatures are higher on the loaded side of the vehicle due to increased loading. Moreover, as the tyre temperatures are related to the sliding speeds and generated frictional forces, the tyres heat up significantly more on the tyres experiencing higher slip angles. This behaviour is more evident on the skid-pad simulation (Figure 14b), where the front tyres are steered at higher values in order to negotiate the much tighter corners (Figure 15b). As a result, the front tyres generate higher slip angles, which improves the front tyre force generation while increasing the sliding speeds at the tyre contact patches. In addition, the aerodynamic downforce acting on the tyres are significantly less during this event, compared to the high speed lane change manoeuvre, which distributes the vertical loads more evenly between front and rear tyres, as shown in Figure 16. Moreover, the vehicle's roll balance is slightly biased toward the front, which increases the weight transfer on the front end of the vehicle compared to the rear.

During the skid-pad simulation, the vehicle initially completes two right turns which increase the temperature of all the tyres. However, as the vehicle goes into the transition for the left turns and then negotiates two complete left turns, the temperature on the

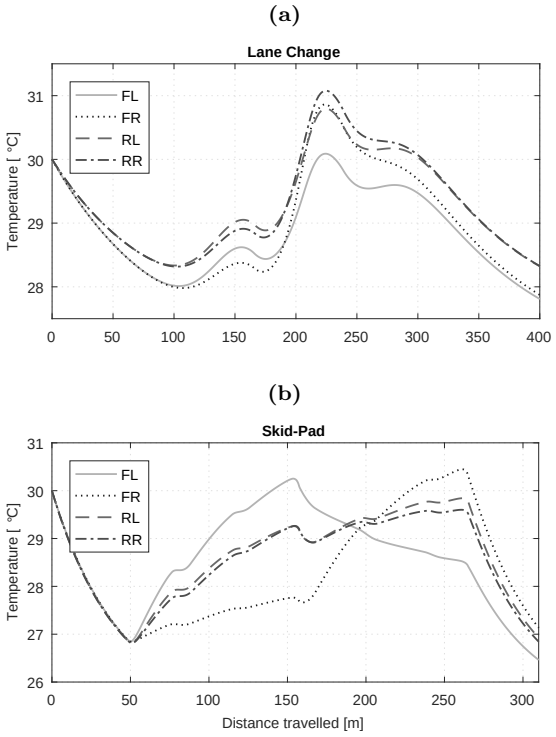

Figure 14: Simulated tyre tread surface temperatures for lane change manoeuvre (a) and skid-pad event (b).

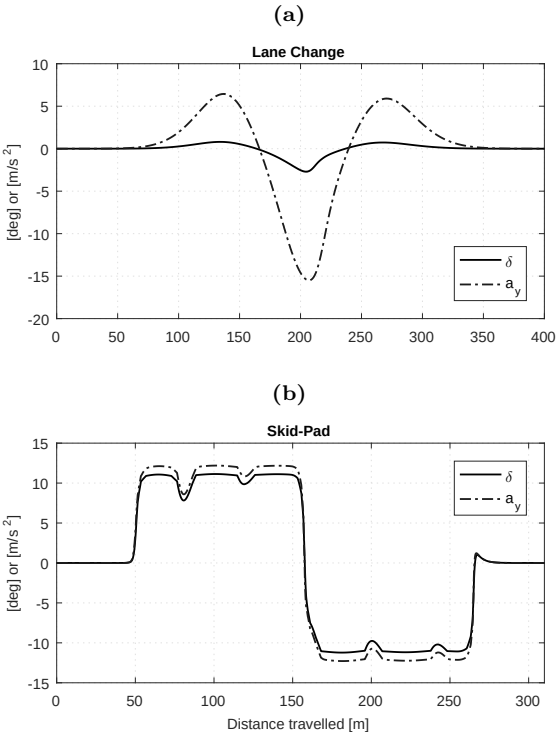

Figure 15: Simulated steering control (δ) input and lateral acceleration (a_y) response for lane change manoeuvre (a) and skid-pad event (b).

front left tyre drops slightly, while other tyres keep on heating up at different rates. For instance, the front right experiences the highest temperature rise rate, as a consequence of higher vertical load and slip angle. The simulated slip angles are shown in Figure 17.

Unfortunately, the studied manoeuvres do not impose a great amount of tyre temperature variations due to assumed simplifications, and hence do not allow for a quantitative analysis of tyre temperature effects on the vehicle performance. However, the qualitative analysis is in agreement with the expected behaviour. Additionally, even though the variation is small, the changing tyre temperatures and resulting lateral force output of the tyres show that the vehicle does not achieve pure steady-state cornering phase, and the driver model needs to make adjustments in steering in order to stay on the desired path. In order to study this effect in more detail, the steering is applied as a constant step input that generates increased tyre temperatures and significant variation in vehicle behaviour. The forward velocity was set to 14 m/s for this simulation. Figure 18 shows the vehicle trajectory where the vehicle initially has a greater turn radius but with time it reduces and becomes steadier. This is directly related with the tyre temperatures (Figure

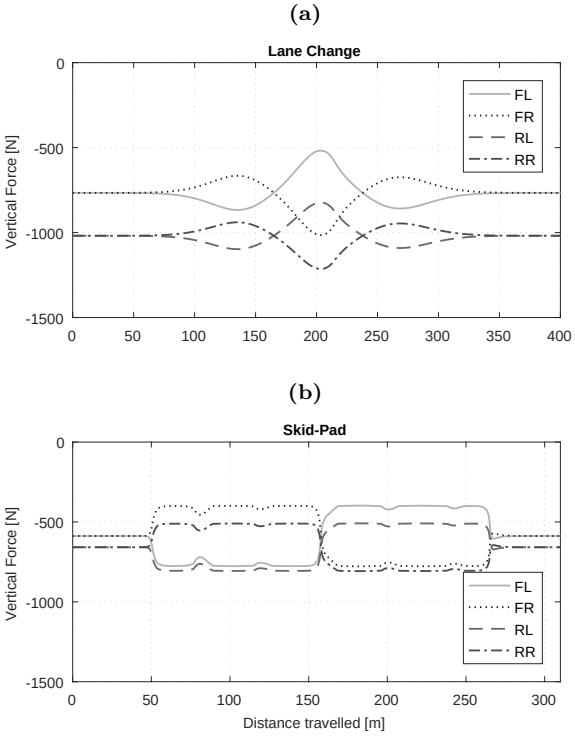

Figure 16: Simulated tyre vertical forces for lane change (a) manoeuvre and skid-pad event (b).

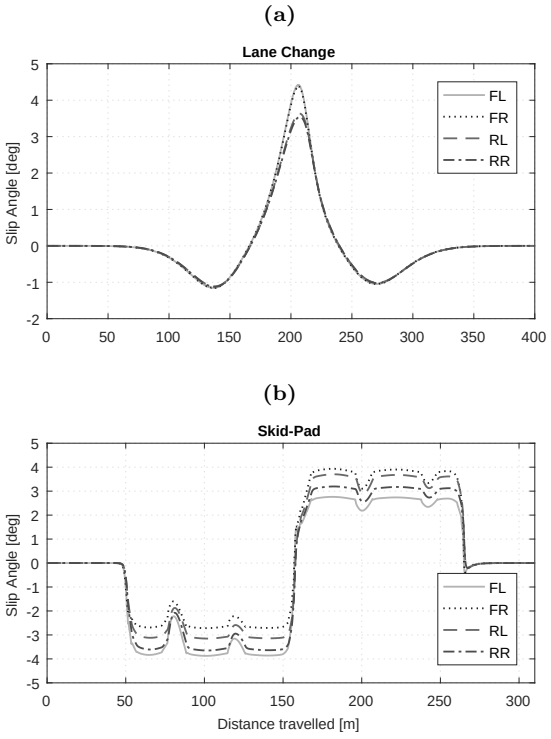

Figure 17: Simulated tyre slip angles for lane change manoeuvre (a) and skid-pad event (b).

19), and as the tread temperatures increase the vehicle's lateral acceleration capabilities increase too until the tyre temperatures reach their equilibrium point or get a steadier behaviour under the current operating condition (Figure 20).

According to the resulting simulations, the point at which the vehicle response is expected to become shallow is after about 20 seconds and the pure steady-state behaviour requires a significant amount of time or until all tyres reach their equilibrium point. However, in reality the effects of the tyre wear are also expected to influence this behaviour dramatically, therefore it is unlikely that the vehicle will ever experience pure steady-state behaviour.

Moreover, investigating the vehicle cornering capabilities with the influence of tyre temperatures, applying a sinusoidal type steering input with constant rate shows that the vehicle is able to corner at higher lateral acceleration with the increase in tyre temperatures experienced during this test. Figure 21 shows the yaw moment against lateral acceleration capability of the vehicle at different averaged front tyre temperatures. As the front tyre temperatures increase, the vehicle is shown to generate higher lateral acceleration while manoeuvring.

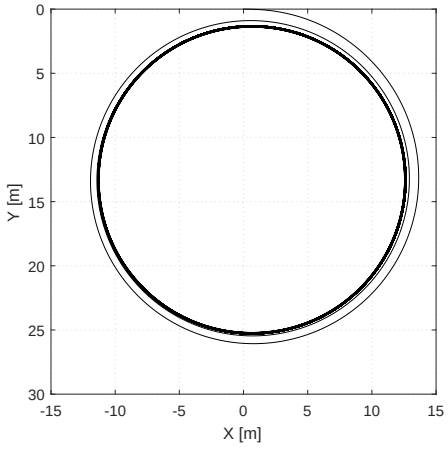

Figure 18: Vehicle trajectory in constant radius steady-state cornering simulation.

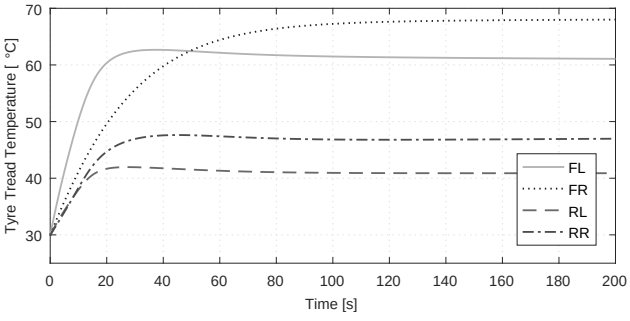

Figure 19: Tyre tread temperature variation in steady-state cornering simulation.

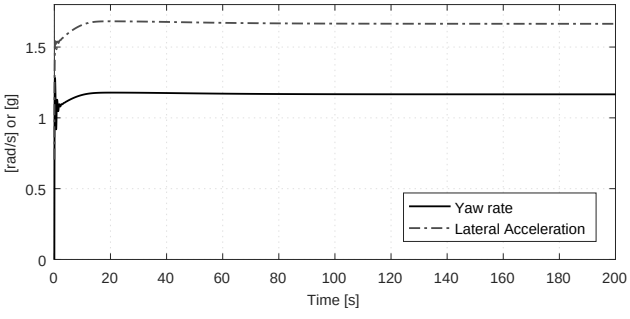

Figure 20: Yaw rate and lateral acceleration profile of vehicle in steady-state cornering simulation.

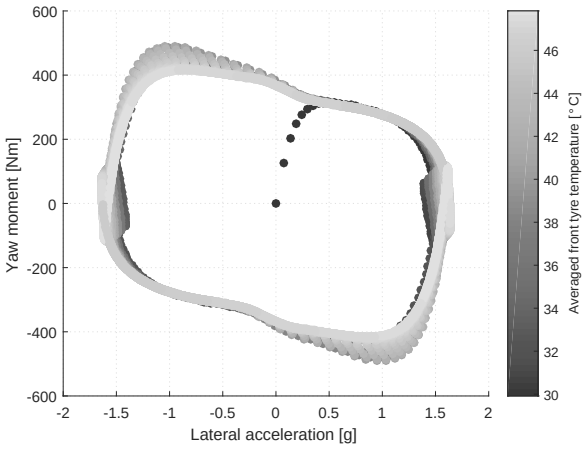

Figure 21: Yaw moment diagram with the influence of tyre temperatures.

Conclusions

In this paper, a unique application of tyre modelling methods for a Formula SAE type vehicle has been demonstrated, which consequently provides a potential tool for improved understanding of the vehicle behaviour.

The combination of existing elements of the simple brush tyre model and newly introduced elements resulted with the introduction of a steady-state physical-based tyre model and a time-dependent, thermo-physical model. Even though utilising mostly simple methods and relationships, estimation of both of the tyre models showed reasonably good agreement with an industry-standard tyre model, and more importantly with the experimental tyre test data. For instance, the introduction of a new approach to account for the load-dependent tread element stiffness provided a good improvement over the existing rigid-carcass type brush tyre models with constant bristle or carcass stiffness. In addition, the unique vertical stiffness description as introduced in the tyre models improved the brush model's ability to respond better to a variety of operating conditions that the tyres are expected to experience while manoeuvring. It is also shown that the temperature primarily effects the frictional behaviour of the tyre and secondarily the stiffness characteristics of the tyre response. On the other hand the thermal behaviour of the tyre model requires further investigation, especially with lower and higher vertical loading conditions, as the thermo-physical model was observed to provide a poor correlation against the experimental data under such conditions.

The implementation of the tyre models in transient vehicle simulation was also found to be relatively straight-forward and highly efficient as the proposed tyre model has shown that it has the ability to realistically replicate the thermal behaviour of the tyres during vehicle manoeuvring. Moreover, both tyre models were also found to require low computational effort. The analysis of vehicle simulation showed that the tyre temperatures significantly and immediately affect the vehicle's cornering capabilities. Furthermore, it is also observed that the vehicle requires a settling time until it can achieve steady-state manoeuvring as the tyres are observed to require a certain time until they reach their equilibrium temperatures.

Funding

This research received no specific grant from any funding agency in public, commercial or not-for-profit sectors.

Declaration of conflict of interest

The authors declare that there is no conflict of interest.

References

Avon Motorsport (2015) *Resource Centre: Formula Student Spring Rate Data.* Available at: `http://www.avonmotorsport.com/resource-centre-downloads` (Accessed: 5 June 2015).

Brayshaw, D. (2004) *The use of numerical optimisation to determine on-limit handling behaviour of race cars.* PhD Thesis. Cranfield University.

Formula SAE Online (2016) *2016 Formula SAE Rules.* Available at: `http://www.fsaeonline.com/content/2016_FSAE_Rules.pdf` (Accessed: 20 April 2016).

Gim, G. (1988) *Vehicle dynamic simulation with a comprehensive model for pneumatic tires.* PhD thesis. The University of Arizona.

Grob, M., Blanco-Hague, O. and Spetler, F. (2015) 'TameTire's testing procedure outside Michelin', *Proceedings of the 4th International Tyre Colloquium: Tyre Models for Vehicle Dynamics Analysis.* University of Surrey, Guildford, United Kingdom, 20-21 April. pp. 31-40. Available at: `http://epubs.surrey.ac.uk/807823/` (Accessed: 9 June 2015).

Kasprzak, E.M. and Gentz, D. (2006) 'The Formula SAE Tire Test Consortium - tire testing and data handling', *SAE International Technical Paper*, 2006-01-3606, doi: 104171/2006-01-3606.

Kelly, D.P. and Sharp, R.S. (2012) 'Time optimal control of the race car: influence of a thermodynamic tyre model', *Vehicle System Dynamics: International Journal of Vehicle Mechanics and Mobility*, 50(4), pp.641-662. doi: 10.1080/00423114.2011.622406.

Kim, S.J. and Savkoor, A.R. (1997) 'The contact problem of in-plane rolling of tires on flat road', *Vehicle System Dynamics: International Journal of Vehicle Mechanics and Mobility*, 27(1), pp.189-206. doi: 10.1080/00423119708969654.

Mavros, G. (2009) 'Tyre Modelling: Current state-of-the-art, future trends and loose ends'. *Vehicle Dynamics and Control Seminar*. University of Cambridge, Cambridge, United Kingdom, 2 April. Available at: `http://www2.eng.cam.ac.uk/~djc13/vehicledynamics/downloads/VDC2009_Mavros.pdf` (Accessed: 4 March 2015).

Mizuno, M., Sakai, H., Oyama, K. and Isomura, Y. (2005) 'Development of a tyre force model incorporating the influence of the tyre surface temperature', *Vehicle System Dynamics: International Journal of Vehicle Mechanics and Mobility*, 43(1), pp. 395-402. doi: 10.1080/00423110500140187.

Ozerem, O. (2014) *Tyre model estimation using simple testing methods*. BEng Dissertation. Oxford Brookes University.

Pacejka, H. B. (2012) *Tire and Vehicle Dynamics*. 3rd edn. Oxford: Butterworth-Heinemann.

Pacejka, H.B. and Sharp, R.S. (1991) 'Shear Force Development by Pneumatic Tyres in Steady State Conditions: A Review of Modelling Aspects', *Vehicle System Dynamics: International Journal of Vehicle Mechanics and Mobility*, 20(3-4), pp.121-176. doi: 10.1080/00423119108968983.

Sharp, R.S., Casanova, D. and Symonds, P. (2000) 'A mathematical model for driver steering control, with design, tuning and performance results', *Vehicle System Dynamics: International Journal of Vehicle Mechanics and Mobility*, 33(5), pp.289-326.

Sharp, R. S., Gruber, P. and Fina, E. (2015) 'Circuit racing, track texture, temperature and rubber friction', *Proceedings of the 4th International Tyre Colloquium: Tyre Models for Vehicle Dynamics Analysis*. University of Surrey, Guildford, United Kingdom, 20-21 April. pp. 21-30. Available at: `http://epubs.surrey.ac.uk/807823/` (Accessed: 9 June 2015).

Smith, N.D. (2003) *Understanding parameters influencing tire modelling*. Report. Colorado State University.

Sorniotti, A. (2009) 'Tire thermal model for enhanced vehicle dynamics simulation', *SAE International Technical Paper*, 2009-01-0441, doi: 104171/2009-01-0441.

Sorniotti, A. and Velardocchia, M. (2008) 'Enhanced tire brush model for vehicle dynamics simulation', *SAE International Technical Paper*, 2008-01-0595, doi: 104171/2008-01-0595.

Appendix I

Notation

a	Half contact patch length
a	Distance from front axle to centre of gravity
a_y	Vehicle lateral acceleration
A_{cp}	Contact patch area
b	Half contact patch width
b	Distance from rear axle to centre of gravity
$C_{F\alpha}$	Tyre cornering stiffness
$C_{F\kappa}$	Tyre longitudinal stiffness
C_{cp}	Tyre friction reduction factor
c_p	Specific heat capacity
F_x	Longitudinal tyre force
F_y	Lateral tyre force
F_z	Vertical tyre force
h	Heat transfer coefficient
K_z	Tyre vertical stiffness
k_p	Bristle stiffness per unit length
K_y	Lateral stiffness of the tyre
l_{cp}	Contact patch length
m	Mass
P_{cp}	Global contact patch pressure
P_i	Tyre inflation pressure
q_x	Longitudinal contact force per unit length
q_y	Lateral contact force per unit length
q_z	Contact patch vertical load distribution
r	Vehicle yaw rate
R_0	Tyre unloaded radius
u	Longitudinal vehicle centre of gravity velocity
u	Longitudinal bristle deflection
v	Lateral vehicle centre of gravity velocity
v	Lateral bristle deflection

V	Velocity
V_s	Tyre slip or sliding velocity
w_{cp}	Contact patch width
x_t	Contact adhesion to sliding transition point
α	Lateral slip angle
γ	Tyre camber angle
δ	Wheel steered angle
δ_z	Tyre vertical deflection
η	Tyre efficiency
κ	Longitudinal slip
λ_g	Vertical stiffness camber coefficient
λ_i	Vertical stiffness inflation pressure coefficient
λ_{av}	Vertical stiffness angular velocity coefficient
μ_k	Kinetic friction coefficient
μ_s	Static friction coefficient
σ_c	Theoretical combined slip
σ_x	Theoretical longitudinal slip
σ_y	Theoretical lateral slip
τ_y	Tyre lateral relaxation length
ψ	Vehicle yaw angle
ω	Tyre angular velocity

Subscripts

a	Ambient
c	Carcass
i	Inflation gas
k	Kinetic
r	Road
s	Static
t	Tread
v	Vehicle
x	Longitudinal direction
y	Lateral direction
z	Vertical direction

Abbreviations

CG	Centre of gravity
FL	Front left
FR	Front right
FSAE	Formula SAE
FSTTC	Formula SAE Tire Test Consortium
MF	Magic Formula
PM	Physical model
RL	Rear left
RR	Rear right
SAE	Society of Automotive Engineers (formerly)
TPM	Thermo-physical model